EasyChair Preprint

№ 11296

# Deep Learning Routes to Thyroid Ultrasound Image Segmentation; a Review

Jatinder Kumar, Surya Panda and Devi Dayal



November 15, 2023

# Deep Learning Routes to Thyroid Ultrasound Image Segmentation; A Review

Jatinder Kumar[1, a)], Surya Narayan Panda[2, b)], Devi Dayal[3, c)]

[1]Department of Computer Science and Engineering, Chitkara University, Punjab, India
[2]Department of Computer Science and Engineering, Chitkara University, Punjab, India
[3]Endocrinology and Diabetes Unit, Department of Paediatrics, PGIMER, Chandigarh, India
[a]kumar.jatinder@pgimer.edu.in
[b]snpanda@chitkara.edu.in
[c]drdevidayal@gmail.com

On the forward-facing of the neck, the thyroid gland yields hormones which support in regulating the digestion. Thyroid problems are most typically detected and classified via ultrasound (US) imaging. US imaging has become one of the most important contributions for analyzing thyroid disorders due to its safety, accessibility, non-invasiveness and cost-effectiveness. Machine learning (ML) advances, especially deep learning (DL) are proving to be beneficial in recognising and quantifying patterns in clinical images. At the heart of these advancements is DL algorithms' ability to extract hierarchical feature representations directly from images, eliminating the requirement for constructed features. This study describes the evolution of ML, the concepts of DL algorithms, and an overview of successful applications, including clinical picture segmentation for US imaging of thyroid-related illnesses. Finally, certain research difficulties are mentioned along with future enhancements.

***Keywords: Deep Learning, Ultrasound Image, Segmentation, Thyroid.***

## Introduction

The thyroid's primary job is to control the body's metabolism through thyroid hormone. Thyroid abnormalities can be caused by a variety of conditions. Medical pictures can be used to detect these anomalies.Ultrasonography can be used to diagnose thyroid problems. Medical image segmentation is an important tool for determining a body's shape and structure on the basis of clinical images. The endocrine system is made up of glands generating hormones that influence the growth and development of the fetus, puberty, level of energy and mood. To ensure that the child's body works properly, these glands need to release exactly the right amount of hormones into the bloodstream. Figure 1 indicates the body's main endocrine organs. Growth disturbances (short or high stature), thyroid issues, adrenal insufficiency, pubertal development disorders, sex development disorders and pediatric diabetes etc. are the different problems that arise due to endocrinological anomalies.

The thyroid gland is an endocrine gland that harvests double thyroid hormones which are triiodothyronine (T3) plus thyroxine (T4). Together T3 plus T4 hormones control variety of metabolic activities including heat production, carbohydrate intake, protein intake, and fat intake. The pituitary gland controls the making of T3 and T4 hormones. When thyroid hormone is necessary, the pituitary gland discharges thyroid stimulating hormone (TSH),

which voyages via the bloodstream to spread the thyroid gland. These hormones are produced by the thyroid gland and go through the circulation to all other organs, regulating metabolism and development. The thyroid gland is responsible for breathing, blood transmission, stomach movements, temperature regulation, muscle function, digestion, and brain function. Abnormalityof thyroid gland can have an impact on the human body's regular physiological functioning.

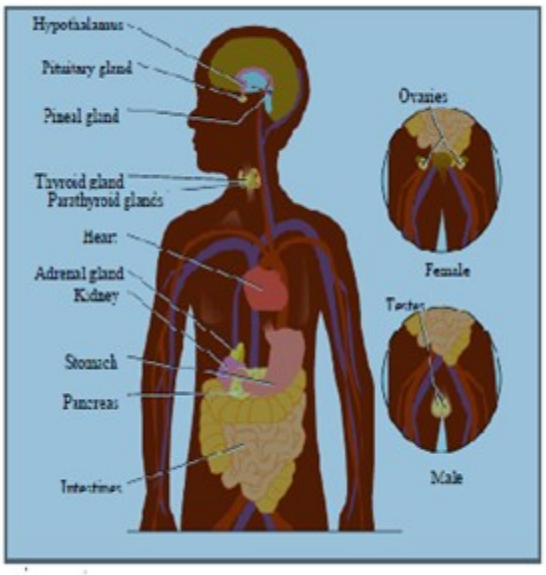


Fig. 1: Endocrine System

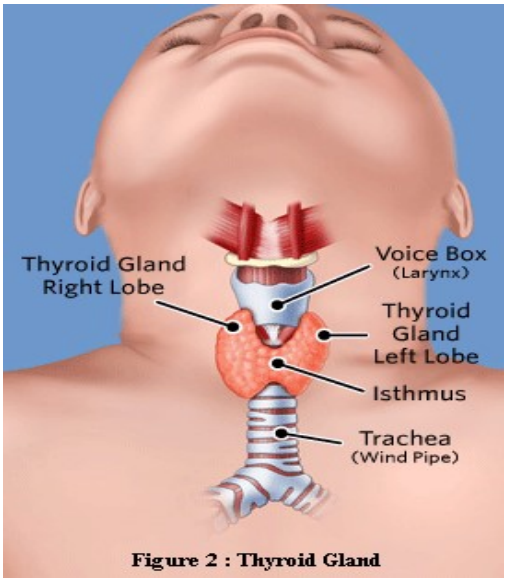


Fig. 2: Thyroid Gland

There are two side lobes on the thyroid, linked in the center by a bridge (isthmus) as shown in figure 2. The upper and lower bilateral thyroid arteries, as well as a small artery known as the thyroid artery, supply blood to the thyroid gland. T4 is responsible for 90% of hormone development, while T3 is responsible for the remaining 10%. Thyroid hormone release is regulated by the thyroid releasing hormone (TRH) and TSH stimulatory activity of the hypothalamic pituitary thyroid axis. Hyperthyroidism (excess thyroid hormone), hypothyroidism (insufficient thyroid hormone), benign (noncancerous), malignant (cancerous), and abnormal thyroid function tests without clinical symptoms are the five basic types of thyroid illness. Hypothyroidism causes weariness, mental fogginess, and absent-mindedness, as well as peculiar cold feelings, constipation, dry skin, fluid loss, nonspecific muscle and joint aches and stiffness, severe or continuous menstrual bleeding and melancholy. Hyperthyroidism is characterised by excessive swelling, heat aversion, increased bowel motions, tremor, uneasiness, anxiety, great heart degree, weightiness, fatigue, impaired attention, unpredictable plus insufficient menstrual flow (2). The types of thyroid diseases and their symptoms are summarize in table 1.

The supreme common endocrine condition in children worldwide is thyroid disorders. Pediatric thyroid disorders (PTD) are a category of hypothyroidism, hyperthyroidism, thyroid nodules and malignancies, and endemic goiter diseases of the thyroid gland in regions with iodine deficiency. Hypothyroidism accounts for about 90% ofPTD, which may also be caused by congenital or acquired causes. Hyperthyroidism is

attributed in large part to Grave's disease. While PTD is single most common endocrine ailments among children, it is also one of the most difficult to diagnose, due to lack of substantial epidemiological evidence, the exact burden of these disorders is unknown.

Table1: Related Works on Segmentation of US Thyroid Image

| **Thyroid Disease** | **Symptoms** |
|---|---|
| Hypothyroidism | Low function caused by not having enough free thyroid hormones. Poor capacity to endure icy, a sentiment tiredness, clogging, gloom and weight increase. |
| Hyperthyroidism | High function caused by having enough free thyroid hormones. Muscle weakness, sleeping problems, a fast heartbeat, heat intolerance, diarrhea and weight loss etc. |
| Structural abnormalities | Structural abnormalities, most commonly a goiter (enlargement of thyroid gland). |
| Tumors | Tumors which can be benign (non cancerous) or cancerous. Lumps that are not normal in the thyroid gland and can be solids, liquids (cystic) and a combination of both (complex cystic). |
| Subclinical Hypo /Hyper thyroidism | Abnormal thyroid function tests without any clinical symptoms (Subclinical hypothyroidism or hyperthyroidism). |

Congenital hypothyroidism occurs in 1:3,000 to 1:4,000 live births, while in the pediatric population; acquired hypothyroidism has a frequency of 1-2%. In girls, thyroid cancer accounts for 6% of all cancers and 1.8% of all thyroid cancers. In addition, even though the global prevalence of iodine deficiency disorders has decreased from 13.1% to 3.2% over the past 25 years, as measured by total goiter levels, it still constitutes a major thyroid problem even in developed countries. In the United States alone, an estimated 4.8 million newborns are predicted to be affected by iodine deficiency with its effects of life-long productivity losses. Collectively, therefore, PTD is a major burden of illness in children and adolescents (3-5). In terms of their relative prominence, ease of prediction and accessibility to medical care, thyroid diseases differ from other endocrine disorders. Thyroid function tests and imaging techniques, such as USand thyroid scintigraphy, are used to diagnose thyroid disorders. The US images are used to determine the cause of hypothyroidism or hyperthyroidism. For example, in patients with hypothyroidism due to Hashimoto's disease, the US shows features of heterogeneousecho texture and hypo-echogenicity, whereas in cases of Grave's disease, there are features of hyper vascular.

A branch of computer science that makes an effort to make PCs smarter is Artificial Intelligence (AI). Incorporating intelligence into an aspect of interest is one of the necessary necessities for any intelligent actions. A large part of scholars these days accept that without learning intelligence, there is no intelligence. Since the very beginning, ML structures have been used to test scientific information units. Recognition of ML and statistical patterns is the most important discipline in biomedical society because they advocate assurance to increase the sensitivity and precision of discovery and diagnosis of an ailment, even though the objectivity of choice making mechan nism is defined. In clinical science, diagnosis is a big challenge since it is important in deciding

whether or not a patient has the disease which assists to define the effective course of treatment for the diagnosed disorder. A hot research field of computer science has been the application of techniques for disease diagnosis using intelligent algorithms (6).

A history and physical examination are used to establish a diagnosis. Thyroid disease is diagnosed based on symptoms and the presence or absence of a thyroid nodule. A blood test and USinvestigation will be given to the majority of patients. A biopsy or radioiodine scanning and uptake studies may be required in some cases. The appropriate interpretation of thyroid data, in addition to clinical examination and complementary investigation, is a fundamental challenge in the diagnosis of thyroid disease. A number of deep learning algorithms were used to provide the best outcomes in US thyroid images. The many stages of image processing are represented in Figure 4.Most image processing systems include steps such as picture preprocessing or enhancement, segmentation, feature extraction, feature selection, and classification.

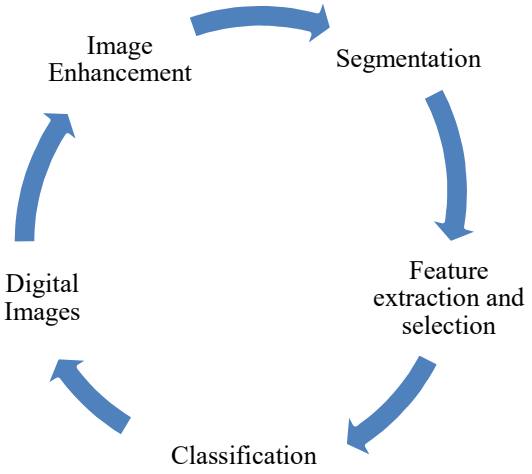


Fig. 3: Phases of Medical Image Processing

Preprocessing is the initial step in image processing. It must be performed on digitized images in order to remove noise and increase image quality. The goal of the segmentation process is to identify suspicious zones of interest that include anomalies. The features are calculated utilising the properties of the region of interest during the feature extraction stage (ROI). The feature selection stage, in which the smallest collection of features is picked, is a major challenge in algorithm design. The process of picking a smaller feature subset that produces the highest value of a classifier performance function is known as feature selection. Finally, a categorization is accomplished based on the concept of selected features.

The term "segmentation" refers to the division of an image into several parts. An image is separated into subparts according to the system's requirements in image dissection. Increase visualisation is main objective of dissection for detection procedure so that it may be handled more effectively and efficiently. The motives for medical image segmentations are depicted in figure 5. All of the aspects that influence the analysis of an illness are covered by segmentation. A disease's navigation can be analyzed, diagnosed, quantified, monitored and planned using the segmentation method.

When there is noise in an image, the problem of uncertainty occurs, making image categorization harder. The reason for this is that noise in the image changes the intensity values of pixels.


Fig. 4: Reasons for Medical Image Segmentation

When there is noise in an image, the problem of uncertainty occurs, making image categorization harder. The reason for this is that noise in the image changes the intensity values of pixels. This change in pixel intensity values messes up the image's intensity range homogeneity. Because of motion in the image, blurring effect, and a lack of various characteristics, noise can appear in the image. The challenge of inconsistency within the intensity values of picture pixels is caused by the partial volume averaging problem. As a result, picture segmentation is critical in medical diagnosis systems to deal with uncertainty (7).

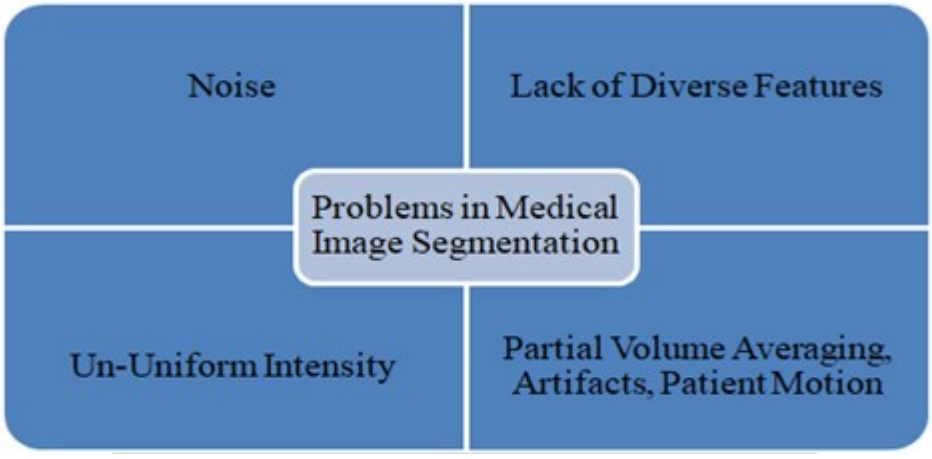


Fig. 5: Problems in Image Segmentation

The exact contour of an object within a picture is provided by segmentation models. In contrast to classification models, which identify what is in an image, and

Detection models, which establish a bounding box around specified things, pixel by pixel information are provided for a given object. Because it allows for non-invasive diagnostic approaches, clinical picturing are significant quantity of present healthcare system. This involves making pictorial and practical depictions of the human body's internal and organs for therapeutic research. X-ray established procedures resembling regular X-ray, computed tomography (CT), and mammography, in addition to molecular scanning, magnetic resonance imaging (MRI), plus ultrasonic scanning, are among the various varieties. Apart from these medical scanning modalities, medical scanning are progressively applied for diagnosing a variety of illnesses, notably individuals involving skin and thyroid (8). There are two parts of medical images; 1) Reconstruction and image development; 2) Image analysis and processing (9). Picture formation is the procedure of physically and visually projecting three-dimensional (3D) section points into two-dimensional (2D) picture level positions. Iterative reconstruction refers to iterative approaches used for specific scanning methods to rebuild 2D and 3D pictures. While iterative algorithms are used in image reconstruction, iterative reconstruction known to iterative approaches used in specific scanning methods to rebuild 2D and 3D images. A picture must be reconstructed from object projections in computed tomography, for example. Picture handling is the procedure of applying actions to a picture in order to increase it or extract vital information.

Obtaining photos has become easier as technology advances, enabling for the bulk creation of high-resolution images at incredibly low costs. As a result, image processing algorithm development in the US has substantially improved. As a result, systems for extracting useful information from images have been created using automatic picture analysis or assessment. The first stage in automated image analysis is segmentation, which splits the image into visually different parts with semantic meaning for the situation at hand. Each of these areas usually has similar features in relations to grey equal, quality and shade (10). For further analysis, such as determining texture homogeneity levels or layer thickness, clear segmentation and identifiable sections are required (11). Figure 7 depicts three categories in which image segmentation techniques can be characterized.

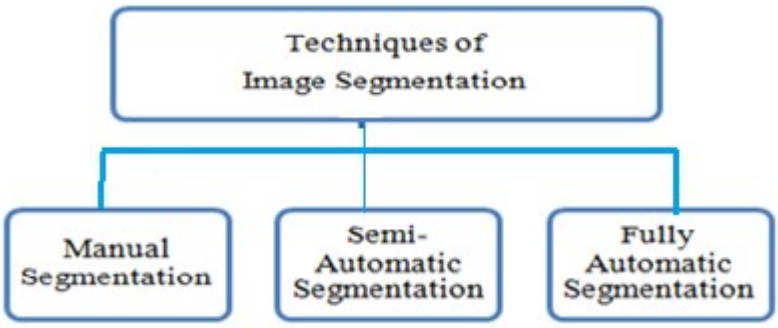


Fig. 6: Image Segmentation Techniques

The radiologist must first define the region of interest (ROI) which plot correct margins around the ROI before using MS methods to correctly mark each pixels of clinical picture. Manual segmentation was vital because that gives annotated ground truth pictures that may be used to construct semi-automated and fully automated segmentation approaches. MS is sluggish to process and is only suitable for small image databases. Due

to the lack of a distinct boundary (low contrast) in high resolution pictures, little deviations in the choice of pixels for the ROI margin can effect in a considerable inaccuracy. Due to the lack of a visible boundary (low contrast) in high resolution images, a slight change in the ROI margin selection can effect in a substantial inaccuracy. Additional disadvantage of physical segmentation is that it is independent, as the method is reliant on the professional's awareness and understanding, and as a result, there is regularly important variation between and within experts (13).

Semi-automatic segmentation strategies utilising automated algorithms require a minimal amount of user input to get effective segmentation results (14). The user may be asked to select an approximate beginning ROI, which will then be utilised to segment the entire image. To reduce segmentation error, it can necessitate physical verification and removal of region margins. Techniques for semi-automatic segmentation comprise: 1) seeded region growth (SRG) method, which combines neighboring pixels with like intensities iteratively established on a user-supplied first seed idea; 2) Iteratively altering initial boundary forms represented by contours utilising a shrinkage or expanding procedure established on the implied level of a utility using a level set established active contour model, which has the advantage of requiring no prior shape information or initial ROI locations and 3) localised area-based active contour approaches, which use region parameters to characterise the image's foreground and background using small local regions and can handle heterogeneous textures (15-17).

The user is not required to interact with the completely automated segmentation procedures. Shape models, atlas defined segmentation methods, random forest, and deep neural networks are all supervised learning procedures that need drill information. Unsupervised learning techniques require labeled pictures generated through manual segmentation for both training and validation data, incurring the same constraints as previously mentioned. The significant differences in ROI shape, size, texture, and colour, as well as weak contrast between regions, pose additional challenges for automated segmentation of medical images (18).

Big disparities in the source picture data might result from noise in the acquisition of source data, which is prevalent in real-world applications. As a result, maximum current systems established through clustering methods, watershed procedures, and machine learning established methodologies for a fundamental lack in worldwide application, limiting their usage to a small amount of applications. Moreover, social feature trade, commonly used in conjunction through machine learning methods established on support vector machines (SVM) or neural networks (NN), is inefficient, fails to handle regular material in its fresh usage, and does not classically adapt to fresh evidence. Deep learning algorithms, may be able to process raw data without the requirement for predefined features. Natural image segmentation for semantic reasons, as well as biological image segmentation, have all been effectively accomplished using these methods (19). Quicker central processing units (CPUs) and graphic processing units (GPUs), which substantially concentrated exercise, performance times, along with access to huge datasets and progressions in learning methods, have supported the rise in use of deep learning systems (20).

The following is a breakdown of the review's structure. In Section 2, we'll cover AI and several related technology approaches, as well as the machine learning method for picture dissection and its designs, common deep learning architecture engagement methods, and image segmentation performance measures. Section 3 discusses latest work with deep learning prototypes for diverse biological picture segmentation applications. The problems of deep learning-based picture segmentation, conclusion, as well as future study fieldsare discussed in section 4's.

## Deep Learning Overview

### Artificial Intelligence (AI)

In general, artificial intelligence (AI) is described as the use of any equipment to simulate the human cognitive process, which includes learning, applying, and solving difficult problems. Figure 8 shows the hierarchical links between AI, an area of computer science that comprises ML, DL and convolutional neural networks (CNNs). AI, dubbed "the fourth industrial revolution", is significantly transforming the terrain of our entire lives today. The phrase "artificial intelligence" was initially proposed during a symposium at Dartmouth in 1956 and its evolution shown in figure 9.The successful development and deployment of image classifiers since 2012 has contributed to AI's current resurrection.Importantly, AI approaches are highly suited to imaging-based domains since the image itself is the primary source of data for training AI algorithms because pixel values can be quantified [21-23].

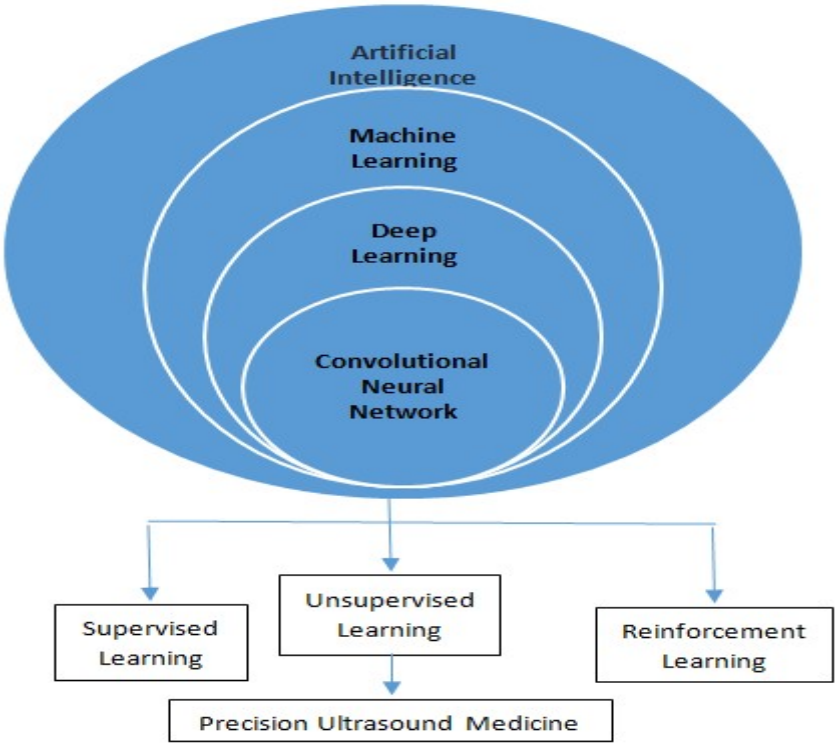


Fig. 7: The Hierarchical Relationships of AI, ML, DL and CNN.

## Machine Learning (ML)

Machine learning established picture dissection method which frequently used for categorizing ROI, such as unhealthy or healthy regions. Preprocessing, which can include the usage of a filter to eliminate blare or for the purpose of distinction improvement, is the initial step in constructing such an application. The image is segmented after it has been preprocessed, utilising techniques such as thresholding, clustering, and edge-based segmentation. Color, texture, dissimilarity and dimension features are extracted from the ROI after segmentation. Using feature selection procedures like principal component analysis (PCA) or statistical analysis, the dominant qualities are consequently determined. The proposed topographies are then fed into an ML classifier such as SVM or NN. The ML classifier identifies the best border between each class by combining the response feature vector with the aim class labels [24].

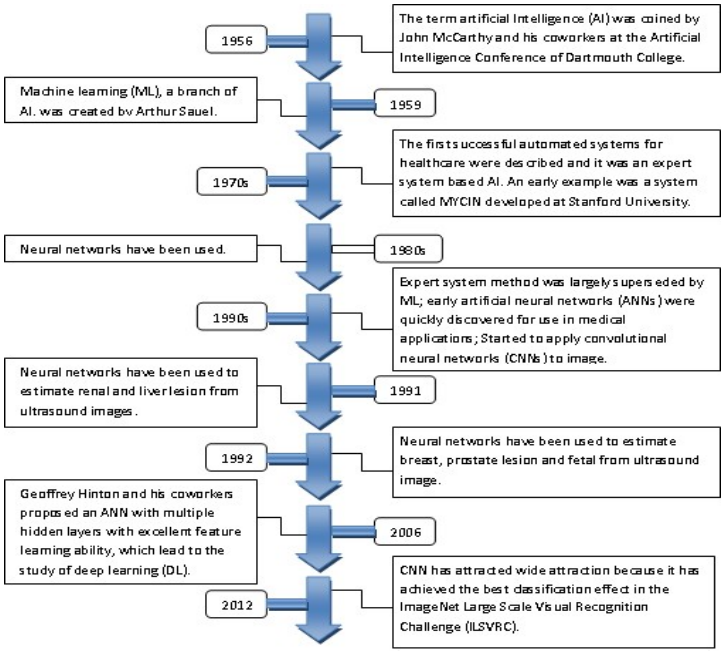


Fig. 8: Evolution of Machine Learning Technology

Subsequently drill, the ML classifier can be used to categorise fresh facts. The right preprocessing required based on raw picture data, defining the suitable features and length of the feature vector which defining the kind of classifier are all common issues. The classifier's type, as well as the relevant qualities and length of the feature vector, are all factors to consider.

## Deep Learning-based Classifier (DLC)

Deep learning which is subdivision of ML that includes computing hierarchical features or depictions of sample facts (for example, photographs) by combining lower level abstract qualities, higher level abstract qualities are formed (25). DLC can process raw images straight, eliminating the necessity of preprocessing, dissection, and feature abstraction. Major DL methods necessitate image scaling due to the input value constraint. Some processes call for force normalisation and contrast enhancement that may be evaded by employing the facts augmentation methods deliberated late in the

passage. As a result, DLC improves classification accuracy by avoiding issues like erroneous feature vectors and sloppy segmentation. The feature vector is fed into a machine learning classifier, which produces the object class, whereas the picture is fed into a deep learning classifier, which produces the object class. It's worth noting that deep learning is theoretically superior to regular artificial neural networks (ANN) because this one has additional layers (26). Representable learning occurs when each layer translates the preceding layer's response facts into a new depiction at advanced and additional abstract level. As a result, the model can learn both local and inter-relationships within hierarchical structure of the data. That all level of a deep learning network, a nonlinear purpose transforms data into representation. In most circumstances, the occurrence or nonappearance of edges in precise arrangements, as well as their location in the image, can be determined using attributes gained from an image's initial layer of representation. The second layer detects edge location while ignoring slight changes, and the third layer combines these patterns into higher groupings that match to sections of comparable matters, allowing subsequent layers to recognise objects using these groupings (27). Deep learning's remaining efficiency for variety of artificial intelligence uses is due to this hierarchical feature representation, which learns straight via response.

The relationship of ML and DLC methodologies is displayed in Figure 10 beneath (28).

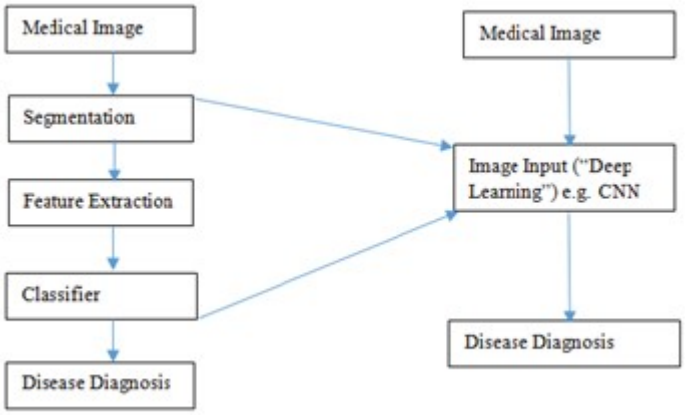


Fig. 9: Relationship of Machine Learning and Deep Learning

## Deep Learning Architecture

### Convolutional Neural Network (CNN)

Because it is similar to standard NN, CNN is the most often used deep learning architecture. Contrasting a traditional NN (displayed in Figure 11), CNN responds to a picture and has a triple dimensional structure of neurons to only connect to a little fraction of the prior level rather than the whole level (displayed in Figure 12). The convolutional layer makes bulks of feature maps comprising the filter's retrieved features by performing a convolution operation among pixels in the response picture and a strainer. The nonlinear activation layer of ReLU which increases nonlinearity and training speed by applying the function f(x) = max (o, x) on reply inputs. Because computations are dependent on surrounding pixels, the pooling layer down samples the response inputs to minimise the spatial dimensionality of the image to lower estimation price to avoid overfitting. It is also conversion in different [29].

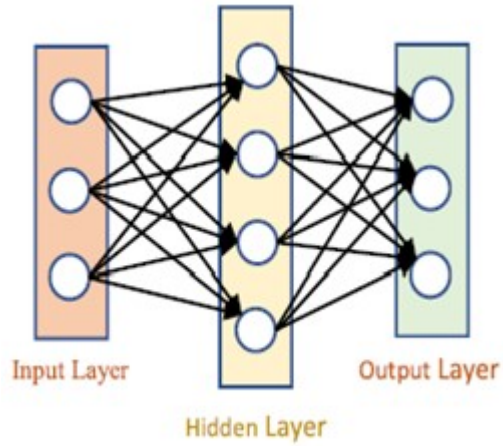


Fig. 10: Traditional Neural Network

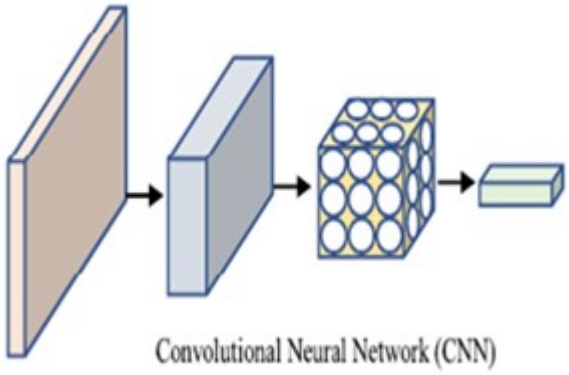


Fig. 11: Convolutional Neural Network

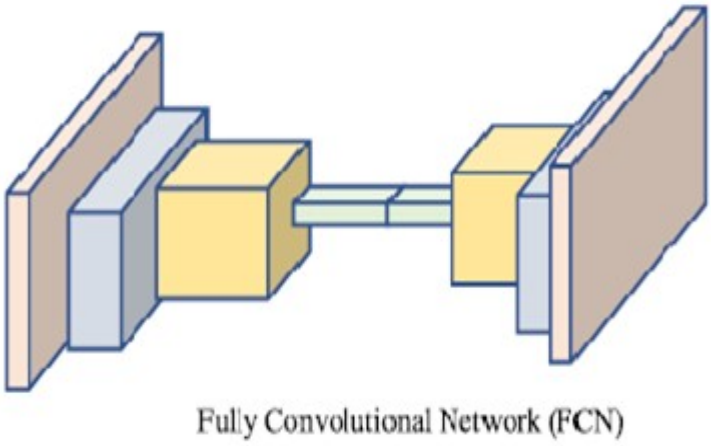


Fig. 12: Fully Convolutional Network

CNN is frequently used to tackle classification problems, as previously indicated. To practice CNN for semantic dissection, response picture was distributed among minor squares of the identical magnitude. Patch is then progressive to the next pixel in the centre to be classified. However, because the corresponding topographies of the sliding squares are not reprocessed, the image loses spatial information of topographies travel to finishing completely interconnected layers of network which approach is inefficient. To resolve this difficulty, the FCN was suggested (shown in Figure 13).

**Restricted Boltzmann Machines (RBMs)**

RBMs (Restricted Boltzmann Machines) are NN that are based on energy models (EBMs). By attributing scalar energy to each precise configuration of the variables, EBMs encode dependency between variables.

While learning, one energy function is created which produces low energies on behalf of correct residual variable values and higher energies for incorrect values.

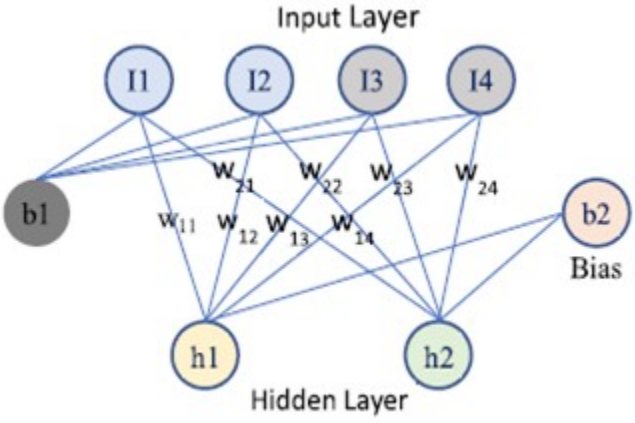


Fig. 13: Restricted Boltzmann Machines (RBMs)

The dominance of the accessible energy functions is determined using the loss function that is minimised during learning.There is no output layer in the RBM. It has lone response layer (I1,..., I4), lone unseen layer (h1, 2), a bias vector (b1, b2), and a weight vector (w). Established with plan displayed in figure 14, the RBM's energy function with ai weighted inputs can be written as:

$$E(I,h) = -\sum_{i} a_i I_i - \sum_{j} b_j h_j - \sum_{ij} I_i h_j w_{ij} \qquad [1]$$

Deep Belief Network (DBN) is a form of RBM created through stacking, in which each layer communicates with the layers above and below it.Undirected connections are found in the first two layers, while directed connections are found in the bottom levels.In contrast, the Deep Boltzmann Machine (DBM) is a form of RBM network that solely comprises undirected connections. Due to noisy existence of responses, DBMs are consideration to handle uncertainty fine.

## Autoencoder based Deep Learning Architectures

The picture is downward sample to obtain a latent representation of smaller dimensions, which allows the autoencoder to be trained and learn on the condensed form of the pictures in autoencoder-based deep learning systems. Figure 15 depicts the design of an autoencoder.

The number of nodes in the unknown layer exceeds the quantity of enter values, which is one of the problems with autoencoders. A null function, in which the productivity equals the response, could be learned by the network. Denoising autoencoders are employed to address this problem, in which the data is decisively corrupted by randomly allocating roughly 45% of the input values to zero. The loss function's output is compared to the original input, removing the possibility of learning a null function

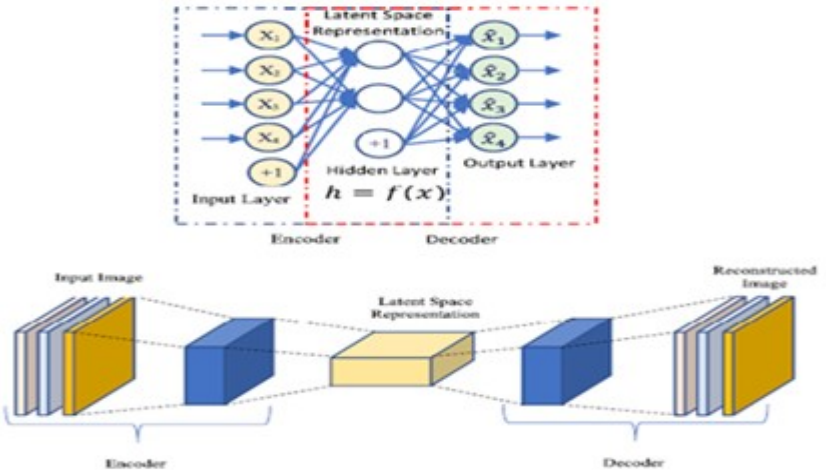


Fig. 14: Autoencoder Architectures with Vector

Because of breaks in latent space depictions, autoencoders have partial applicability and cannot be employed as generative models. To solve this problem, variational autoencoders were created. For a variational autoencoder, the encoder produces two encoded vectors rather than a single encoded vector. The means vector is one, and the standard deviations vector is the other. These vectors are used as inputs to an accidental adjustable that samples productivity encoded vector. Which lets the decoder to successfully decode the encoded data, even if input varies slightly during training. The latent space representation is designed to be continuous because of the autoencoder's stochastic nature, permitting for haphazard interpolation and specimen.

## Sparse Coding based Deep Learning Architectures

Unsupervised learning in which the input data is represented by an overcomplete set of basis vectors is known as sparse coding. The measurement of the latent depiction is larger than the input, which is referred to as overcomplete. The goal is to find a linear mixture for these basis vectors that matches the certain response. Extra sparsity requirements must be added to handle any degeneracy because the network is over completed. Sparse coding offers the benefit of finding correlations between similar descriptors and capturing key visual aspects.

## Generative Adversarial Networks (GANs)

The goal of GANs is to use a neural network to produce a generator that simulates a transform function that receives unplanned variable as response and, once trained, tracks the desired distribution. Simultaneously, a discriminator network is trained to differentiate among generated and real facts. The two networks compete against one another, with one attempting to maximise the ultimate grouping error among produced and actual data and the other attempting to minimise it. As a result, with each iteration of the training method, both networks improve.

## Recurrent Neural Networks (RNNs)

RNNs are intended with function with sequence kind responses when the scale of response not anticipated. The input for the series varies starting various other inputs in

that it has an effect on surrounding values, and the network must recognise this relationship. RNNs are networks that produce current output depending on both current input and learning from previous outcomes. The previous response data is stored in a hidden state vector as part of the network.This means that depending on the previous inputs in the series, the same input might produce different outputs. The network generates distinct fixed-size output vectors when it is repeatedly changed with varied input series values. With each input, the concealed state is updated. To increase the depth of RNNs, additional hidden state layers, non-linear hidden layers among the response and the unknown state layer, more layers among the unknown state layer and the output layer, or a mixture of all three can be added.

## Standard Deep Learning Architecture Implementation Methodologies

Picture segmentation procedures based on deep learning have been applied in a variety of ways. The first method requires the accessibility of a large labelled dataset and is time-consuming because the neural network is created and skilled from scratch. The other strategy, some pre-trained CNNs, such as AlexNet, can be used to classify 1.2 million great tenacity photos for 1000 different classes (30). In this strategy, the last few levels of the network are routinely removed and rebuilt with fresh mission specific layers. In early layers, low-level features learnt from millions of images are mixed with task-specific information acquired in the end layers to create a network for categorising fresh photos. Which give the benefit of saving period during employment because just a minor number of weights must be establish. Transfer learning is more effective than random weight initialization when networks are trained on ImageNet data (31).

The third method involves extracting features from data using pre-trained CNNs and then using those features as responses to train a customary classifier like a support vector machine for classification. This technique has the benefit of being able to extract features automatically for a huge amount of category facts, removing the need for time-consuming human feature abstraction. Two renowned convolutional neural networks are U-Net (32), which was established for biomedical picture subdivision, and V-Net, which was established for volumetric medical image segmentation (33). A U-Net is an FCN with two paths: one for contraction and the other for expansion. The contraction path is made up of successive convolutional layers and a max-pooling layer.

## Biomedical Images Types

Depending on the imaging technology, there are many sorts of biomedical images. Some of the most often utilised biomedical imaging methods are listed below.

## Clinical Photographs

Clinical pictures are computerized pictures of a patient's body use to manuscript wounds, blisters, and skin limitations. These photos could be automatically analysed to monitor therapy efficacy completed period. Clinical photos are commonly recycled in dermatological and aesthetic dealings to pathway earlier and later skin or structural representations. Melanoma, a type of skin cancer, is most typically diagnosed via clinical pictures.

**X-ray Imaging**

X-ray imaging is the best often applied imaging method for detecting fractures and bone dislocations where outcome is a two-dimensional image. In order to develop imaging analysis tools, the National Institutes of Health (NIH) has made 100,000 chest x-ray imagespublic, along with related data and diagnoses [34]. Correspondingly, the Massachusetts Institute of Technology (MIT) has made a dataset of over 350,000 chest x-rays available for evolving machine learning prototypes to perceive 14 common conditions like pneumonia and punctured lung [35].

**Computed Tomography (CT)**

CT which is computed imaging method which creates complete cross-sectional descriptions of the body's internal organs, bones, soft tissue plus blood vessels with 360 grade x-rays.

The slanting plane, which is upright to the body's long axis, is where most photographs are taken. Slices of these photos can be reformatted into many planes and combined for creating triple dimensional pictures. CT resolved biomedical imaging difficulties, it's regularly utilised to identify cancer by detecting tumour presence and size.

**Ultrasound Imaging (US)**

Following the continued emergence of improved ultrasonic technology and the well-established US-based digital health system, US, a versatile green imaging modality, is developing globally as a first-line imaging approach in a variety of clinical sectors. High-frequency linear transducers (7.5-15.0 MHz) are used in the US, which may penetrate to a depth of up to 5 cm and generate high-definition images. US regarded as a potent which widely utilised screening and diagnostic tool for physicians and radiologists as one of the most usually used imaging modalities. Owing to its virtual protection, low price, noninvasive nature, real-time display, operator comfort, and experience, US imaging extensively employed in prenatal screening throughout globe. Several important advantages of US over additional medicinal scanning modalities like X-ray, magnetic resonance imaging (MRI) and CT have been established throughout the decades, including non-ionizing radiation, mobility, approachability, and price effectiveness (36). Many guidelines, including the American Thyroid Association, the American Association of Clinical Endocrinologists and the European Thyroid Association, now recommend US as the first-line imaging modality for detecting thyroid disorders. As a result, various Thyroid Imaging Reporting and Data Systems based on US images have been built in recent years (37 – 40).

### 2.6.5 Magnetic Resonance Imaging (MRI)

In MRI imaging technique a high magnetic fields use to create pictures of physiological progressions, organs, and tissues within the body. Non-bony bodily parts, also known as soft tissues, are imaged using MRI. CT scans and MRI are fundamentally different in that MRI uses ionising radiation. In comparison to x-rays and CT scans, MRI

scans provide better resolution for knee and shoulder problems. The Open Access Series of Imaging Studies (OASIS) programme has compiled neuroimaging datasets with approximately 2000 MRI sessions for biomedical scanning investigators (41).

**Optical Coherence Tomography (OCT)**

In OCT technology a low-coherence light being practice to get micrometer pledge, double plus triple dimensional pictures from within biological tissue. Because OCT gives a cross-sectional image of the retina that allows the practitioner to view each layer clearly, it is regularly used to diagnose eye problems. Layer mapping and wideness assessment are now possible, that was used for conclusion.

**Microscopic Images**

Medical images taken at a microscopic level are utilised to assess the tissue's small structure. Biopsy is utilised to retrieve tissue for investigation, and subsequently staining components are employed to expose cellular features in areas of the tissue. Counter stains are used to give the graphics more colour, visibility, and contrast. This type of imaging is commonly used to diagnose malignancy. On a steady basis, the nucleus plus allocation of cells in the tissue, as well as their form and size, are all tested.

**Scintigraphy**

Scintigraphy, often known as a thyroid scan, is performed in nuclear medicine. Scintigraphy is used to determine the active (functioning) portion of the thyroid gland. The patient is given a radioiodine drug, and then gamma cameras are used to capture photographs of the thyroid and reveal the part of the thyroid that uptakes iodine, i.e. the active or functional component of the thyroid. Scintigraphy imaging is a type of 2-D imaging that is used to examine the thyroid's function.

**Data Augmentation**

The enactment of DL neural networks was determined by handiness of appropriate facts. The difficulty is that training samples are rarely available in adequate amounts, mainly in medical imaging. Facts augmentation, that includes removing a set of reasonable alterations to the samples (e.g., flip, rotate, mirror) in addition augmenting color (grey) values, is the greatest commonly use method for aggregate the extent of the training dataset. The efficiency of data augmentation is examined in a non-clinical research, and the outcomes tell that classic augmentation methods can enrich by up to 7% (42-44). Various data augmentation strategies are used in the lack of real data to generate additional training data from the existing data pool. Data augmentation strategies update image data in a way that preserves the class, and they can include things like: 1) Image translation: in this practice of moving image pixels in single track, either horizontally or vertically, without altering pictures overall dimension; 2) Image flipping: Flipping the image pixels horizontally and vertically by retreating the rows and columns of pixels; 3) Picture Rotation: Rotation of an picture from 0 to 360 degrees; 4) Contrast adjusting: Changing picture illumination levels to train the procedure to accommodate for such distinctions in test shots; 5) Image Zooming: Randomly increase in or out of the picture by adding fresh boundary pixels or using interpolation.

Using nearest-neighbor fill, boundary pixel duplication, averaging, or interpolation, few existing pixels being deleted and fresh pixels being included in most of these techniques. The first four solutions are referred to as inflexible data augmentation strategies since the data shape remains unaltered. The fifth method keeps the vertical and horizontal augmentation ratios the same. If it's not the same, the picture will spread further in single way than the other (image stretching). Goal of these augmentation techniques is to make deep neural networks more generalizable while avoiding feature under-fitting and over-fitting. These strategies are usually applied mechanically throughout the network's training phase. Additional resolution is to transfer knowledge from successful models that have been implemented in the same (or even other) industries. In transfer learning the system trained to recognize and apply understanding educated in a prior origin domain to a fresh assignment. Transfer learning, on the other hand, is influenced by network structure, organ imaging modality, and dataset size (45).

## Quantitative analysis

The objective analysis is a crucial metric for determining whether or not a segmentation algorithm is effective. The efficiency of the picture segmentation system is assessed using well-established benchmarks, allowing the system to be compared to current approaches in the literature. A number of factors, including the system's operation, influence the selection of an appropriate assessment metric. These metrics can be used to examine computational difficulty, handling time, memory usage, and correctness, among other things (46). Table 2 defines the several abbreviations (TP, FP, FN, and TN) applied to evaluate the segmentation performance of deep learning prototypes:

Table 2 : Definition of the abbreviation

| Category | Actual Disease | Actual No Disease |
|---|---|---|
| Predicted Disease | True Positive (TP) | False positive (FP) |
| Predicted No Disease | False Negative (FN) | True Negative (TN) |

## Accuracy

It is the most fundamental performance indicator. Overall pixel precision is another name for it. The accuracy is in determining whether a patient has an illness or is healthy.

$$Accuracy = \frac{Correctly\ Predicted\ Pixels}{Total\ number\ of\ Image\ Pixels} = \frac{TP + TN}{TP + FP + FN + TN} \quad [2]$$

## Precision / Specificity

The fraction of illness pixels in the programmed subdivision outcome that correspond to the ground truth illness pixels is known as precision. Because precision is prone to over-segmentation, it is a valuable benchmark of segmentation performance. The capability to precisely quantify healthy cases is referred to as specificity (47 – 49).

$$\text{Precision} = \frac{Correctly\ Predicted\ Disease\ Pixels}{Total\ number\ of\ Predicted\ Disease\ Pixels} = \frac{TP}{TP + FP} \qquad [3]$$

**DICE Similarity Coefficient (DSC)**

DSC is superior to total pixel accuracy because it reflects equally false alarms and missed data in each class. DICE be too thought toward be real superior since it measures not just the amount of pixels that have been suitably identified, but also the precision with which the segmentation borders have been drawn (50). Here S stands for segmentations in this case.

$$DICE = \frac{2|S_{Ground\ Truth} \cap S_{Automated}|}{|S_{Ground\ Truth}| + |S_{Automated}|} = \frac{2 \times TP}{2 \times TP + FP + FN} \qquad [4]$$

**Sensitivity / Recall**

Sensitivity refers to the ability to accurately measure disease cases. The fraction of illness pixels in the ground truth which are exactly predicted using programmed segmentation is referred to as sensitivity.

$$Sensitivity = \frac{Correctly\ Predicted\ Disease\ Pixels}{Total\ Number\ of Actual\ Disease\ Pixels} = \frac{\text{TP}}{\text{TP} + \text{FN}} \qquad [5]$$

**Jaccard Similarity Index (JSI)**

The percentage of the space of intersection among the anticipated subdivision and the ground fact subdivision to the region of merger among anticipated subdivision and the ground truth subdivision be called JSI (Intersection-Over-Union).

$$JSI = \frac{S_{Ground\ Truth} \cap S_{Automated}}{S_{Ground\ Truth} \cup S_{Automated}} = \frac{TP}{TP + FP + FN} \qquad [6]$$

As can be seen from the above, there is a distinction between JSI and DSC.

$$JSI = \frac{DSC}{2 - DSC} \quad DSC = \frac{2JSI}{1 + JSI} \qquad [7]$$

**Negative Predictive Value (NPV)**

The likelihood that a disease does not exist given a negative test result is defined as (51):

$$NPV(\text{Negative Predictive Value}) = \frac{\text{TN}}{\text{TN} + \text{FN}} \qquad [8]$$

**Literature Review**

A review of various segmentation approaches for thyroid diagnosis using US images done and table 1 presents a summary of recent work in biomedical picture segmentation using deep learning methods. We looked at research that used deep learning

prototypes aimed at biological picture separation. The table contains the editorial orientation, the modality, which describes the picturing methods applied for picture arrangement otherwise acquirement, the style, which describes the deep learning design use for subdivision, the comments part, which in brief describes the planned method, and lastly the performance metrics with brief descriptions used to calculate the planned algorithm. The popular approaches, as shown in table 1, are established on CNN or FCN. No one of these articles practice transfer learning; however one of them does use a deep learning model for feature extraction before classifying the data with a structured support vector machine. US, CT and MR were the most commonly employed imaging modalities in these applications, which reflects the current research orientation. The ease with which image datasets can be gathered through numerous competitions or other publicly available sources is one explanation for this.

Xu et al. (52) Using three orthogonal image planes, the proposed method divide US pictures of the breast into four key tissues: skin, fibro glandular tissue, mass, and fatty tissue. CNN denotes the tissue class of the addressed pixel inside the picture chunk. Accuracy, Precision, Recall, and F1 measure, all quantitative criteria for evaluating segmentation results, all exceeded 80%, signifying the recommended technique is proficient in distinguishing practical tissues in breast US images. The authors concluded that the suggested method has the potential to offer the segmentations needed to aid clinical breast cancer diagnosis and improve imaging in other medical US modes.

Badea et al. (53) scientists used the LeNet CNN design and the Network in Network (NiN) design to categorise blaze photos. The LeNet CNN design was first designed in 1998 for hand written number detection on banknotes.. The multilayer perceptron is a nonlinear function approximator that improves the generalisation capability of the network. The burn picture database had 611 photographs of 53 paediatric patients through a resolution of 1664 × 1248 pixels. Clinical pictures are carefully crop to a dimension of 230 × 240 pixels. Outcome specified modest plan executed fine for binary classification difficulties, but that as the problems became more complicated, performance dropped substantially.

Kaur et al. (54) the ACEW, DRLSE, and LRBAC (Localized Region Based Active Contour) subdivision methods were described. The forefront and backdrop are discussed for minor regions using this strategy. Every point is considered separately in order to optimise the local energy. Every spot was analysed independently near optimise confined power in order to minimise the power compute in its own limited area. Physical initialization of the mask is required, as is manual parameter change. The distance regularisation term and the external energy term are used in DRLSE to drive the contour to the desired edges.

Poudel et al. (55) concluded that ML techniques generate more accurate and efficient segmentation, but they necessitate a large number of tagged datasets and longer training time. According to the authors, 3D U-Net CNN exists an mechanical subdivision technique for 3-D US pictures that uses a decoder to provide full-resolution subdivision and an encoder to analyse whole image by contracting in every succeeding layer. Although it does take additional training time, this technique has the advantage of being able to partition 3D thyroid glands without the usage of handcrafted characteristics. The

CNN prototype has greatest average dice coefficient (DC) of all the segmentation outcomes, at 87.6%. Random forest (RF) and decision tree (DT), which are non-automated segmentation methods, are two other approaches. This approach has a low computing complexity but is sensitive to certain characteristics. The results of the DC, RF, and DT techniques are 86.20 %, 67.00 %, and 86.20 %, correspondingly.

Shenoy et al. (56) have proposed Improvised U-Net for the probable identification of ROI by segmentation. To achieve greater efficiency, two feature maps, high level and low level, have been explored. The use of these two feature maps helps to avoid low resolution. Further, the Improvised U-Net is tested using the standard dataset DDTI in three sections. First, ROI is compared, which demonstrates that existing models have different ROI than ground models because to limited resolution, but our model has a better ROI. The authors compare the model's True Positive Rate and Dice Coefficient, achieving 98.95 and 95.60, respectively. Furthermore, the model outperforms the previous model by 2.51% and 3.36 %, respectively, according to the comparison analysis. Finally, the author found that, while the Improvised U-Net obtains substantial performance when compared to the present model of segmentation, it can still be improved when batch normalization is taken into account.

Garg et al. (57) created a method for generating a classifier that was trained using a supervised learning algorithm; however, the method was only evaluated on a dataset of five photos. In this study, a feed forward neural network was built to segment the thyroid gland region. Image enhancement, feature extraction, Functional Neural Network (FNN) training and arrangement are among the procedures. This technique uses texture as a criterion in image segmentation. Sensitivity and Specificity, which are 89.06 % and 98.90 %, respectively, are used to assess performance.

Frannita et al. (58) analysed US photos to identify thyroid cancer into three categories based on internal content characteristics. The nodular feature can be used to diagnose thyroid cancer. The time it takes a radiologist to diagnose a thyroid nodule is determined by their experience. Automated method is required to eradicate radiologist dependence. This research focuses on exploiting textural cues to categorise thyroid nodules into three groups. A total of 97 thyroid US pictures were used in this study. The suggested method's initial step is pre-processing, which is utilised to improve detection capability. Then, to find the correct nodules, morphological operation and active contour are used. Histogram, GLCM, GLRLM, and lacunarity are used to extract the segmented area. Multilayer Perceptron (MLP) is used to classify the data based on the extracted value. The achieved precision of 98.97 %, kindliness of 98.92 %, specificity of 99.47 %, PPV of 99.05 %, and NPV of 99.50 %. Lacunarity feature was found to be effective in classifying three classes.

Ying et al. (59) researchers observed that using thyroid nodule segmentation in the form of cascaded thyroid nodule convolution, they were able to locate an exact position for nodules in thyroid ultrasound images, as well as its aspect ratio, margin, and figure.. They came to the decision that the aspect ratio and margin form of nodules in thyroid US pictures affect the doctor's opinion. The proposed method not only aids doctors in locating individual nodules, but it also offers indicative information like margin, shape, and aspect ratio of the nodule. The segmentation outcomes of nodules

with sophisticated margin details are not precise enough in the experimental findings, indicating that FCN still has some shortcomings in terms of accurate segmentation and that it is tough to reestablish all details by up-sampling and interpolation.

Table 2: Related Works on Segmentation of US Thyroid Image

| S.No. | Reference | Modality | Method | Remarks | Performance Metrics and Results |
|---|---|---|---|---|---|
| 1 | Xu et al. (2019) (52]) | 3D US | CNN | The proposed method divides US breast pictures into four main tissues: skin, fibro glandular tissue, mass, and fatty tissue; CNN calculates the tissue class of the image blocks' centred pixel. | Accuracy, JSI, Precision, Recall, and F1measure all yielded presentation scores of greater than 80%. |
| 2 | Badea et al. (2016) (53) | Clinical Images | CNN | LeNet plus Network in Network prototypes were applied to classify burn pictures and assess performance, with arrangement correctness for Skin vs Burn and Skin vs Light Burn vs Serious Burn compared. | Accuracy with LeNet is 75.91% for skin vs burn classification plus 58.01% for skin vs light burn vs serious burn classification. Skin vs Light Burn vs Serious burn were classified with a 55.7 % accuracy by NiN. |
| 3 | Kaur et al. (2012) (54) | US & Scintigraphy | ACWE | There is less reliance on the initialization boundary. Physically, the mask must be initialised, and the parameters must be manually tuned. | Precision DC (80%) |
| 4 | Poudel et al. (2018) (55) | 3D US | CNN | Proposed method haveadvantage of being able to segment 3D thyroid glands deprived of the need of handcrafted characteristics, nonetheless it takes longer to learn. | The CNN model produced the greatest average DC of 87.6 %. |
| 5 | Shenoy et al. (2021) (56) | US | U-Net | The Improvised U-Net obtains substantial performance when compared to the present model of segmentation, it can still be improved when batch normalization is taken into account. | True Positive Rate : 98.95 %<br>Dice Coefficient : 95.60 % |
| 6 | Garg et al. (2013) (57) | US | FNN | It was only tested on a dataset of five photos. | Sensitivity 89.06 % and Specificity 98.90 %. |
| 7 | Frannita et al. (2018) (58) | US | CNN | The focus was on dividing the thyroid nodule into three classes using texture features. A total of 97 thyroid US pictures were used in this study. | Accuracy : 98.97%;<br>Sensitivity : 98.92%;<br>Specificity : 99.47%;<br>PPV : 99.05% and<br>NPV : 99.50% |
| 8 | Ying et al. (2018) (59) | US | CCNN | More accurate segmentation results, but with the drawback of requiring artificial marking. | MO (87.00%) |

Xu et al. (60) presented a machine learning-based automatic segmentation solution for breast US images.The automatic segmentation results are visually consistent with humanly segmented ground truth, indicating that the proposed technique can differentiate various tissues from breast US pictures in the same way that clinicians can. The suggested method splits US breast images into four major tissues using three orthogonal image planes: skin, fibro glandular tissue, mass, and fatty tissue. CNN specifies the tissue lesson for central pixel inside the picture block. Truthfulness, Precision, Recall, and F1measure, all quantitative criteria for evaluating segmentation results, all exceeded 80%, indicating that the suggested technique is capable of distinguishing practical tissues inside breast US pictures. An additional measure, the Jaccard Similarity Index (JSI), has a rate of 85.1%.

Ma et al. (61) in this investigation, the scientists deployed dual pretrained CNNs in a thyroid nodule investigative fusion structure. The basic network to analyze lower-level features, as well as a more complex network for researching higher-level abstract features. The dual CNNs that were skilled independently were combined as response to the softmax layer to diagnose thyroid nodules.

Wu et al. (62) used a triple level Deep Belief Network derived using a distinction improved US series to footage, they categorised malignant and benign key lesions in the liver in their paper. Sparse non-negative matrix factorizations are used to extract time intensity curves (TICs) from dynamic CEUS recordings. Based on these TICs, deep learning is used to categorise benign and malignant localised liver lesions. For accuracy, sensitivity, and specificity, quantitative comparisons show that the suggested method beats the compared categorization methods.

Perrin et al. (63) they trained a CNN to distinguish between congenital heart abnormalities using echo cardiographic images from five different paediatric groups. In their work, a CNN adopting a global average pooling strategy achieved a surprise performance improvement in a precise foetus plane recognition challenge.

Yap et al. (64) a patch-based LeNet, a U-net, and a transfer learning technique using a pretrained Fully convolutional network AlexNet were tested for breast lesion revealing having dual datasets of US images. According to the demonstration, deep learning algorithms enhanced the detection efficiency of two US breast images. Experiments have demonstrated that applying the DL technique enhances overall breast lesion detection performance. The Transfer Learning FCN-AlexNet method produced the greatest results for Dataset A, while the suggested Patch-based method produced the finest outcomes for Dataset B, among the various ways examined in this study. For Dataset B, LeNet delivered the best results in terms of FPs image and F-measure. Because they are based on machine learning and each dataset is given its own model, Deformable Part Models (DPM) and deep learning approaches are malleable for particular attributes of any dataset.

Song et al. (65) offered a new multitask cascade CNN architecture which trained for recognising and categorising thyroid nodules in US pictures by involvement mutual properties which are important for well distinguishing benign and malignant nodules, as well as the complicated background. To reach this goal, we need to integrate a multi-

scale layer in our new learning architecture, which will improve the detection performance of thyroid nodules with a wide range of scales. In our extensive testing, our MC-CNN surpassed the unique single shot finding and other single task classification procedures. The purpose of this study, according to the author, was to create a method for accurately and reliably segmenting the prostate clinical target volume in transrectal ultrasonography (TRUS) pictures for brachytherapy. Because of weak or insufficient landmarks or significant artefacts, segmenting these images can be problematic. We developed a method that uses convolutional neural networks (CNNs) to produce accurate segmentations on both easy and difficult images. They offered two ways for improving segmentation accuracy on challenging photos.

Chang et al. (66) for autonomous thyroid segmentation and capacity assessment utilising computed tomography (CT) images, a progressive learning vector quantization neural network (PLVQNN) for reprocessing technique be created. Based on thyroid architecture, the preprocessing approach is utilised for extorting a thyroid glands' ROI and exclude non-thyroid glands. A learning vector quantization neural network (LVQNN) in the PLVQNN segmented each section of a thyroid CT scan. The training propagates uphill and downwards to neighbouring LVQNNs using the initialization settings and constraints from the centre portion. The proposed method may efficiently partition thyroid glands and estimate thyroid volume, according to experimental data.

Gui et al. (67) in medical photos, there are challenges in segmentation due to noise, low contrast, inhomogeneity, fuzzy or partially absent boundaries, and image artifacts. Prior knowledge has been utilized to segment lesions and organs in medical picture segmentation, such as shape priors, texture priors, appearance priors, and statistic priors. The shape prior is a type of segmentation prior knowledge that is often employed. Training and analytical representations of shapes are the two basic methods for obtaining various types of shape priors. The proposed shape restriction, dubbed the isoperimetric constraint, is inspired by differential geometry's well-known isoperimetric inequality. This segmentation technique provides accurate lesion area localization, morphology, and borders.

Mylona et al. (68) proposed innovative assembly for programmed modification of region-based active contour regularization. This method worked for a variety of imaging modalities and did not necessitate prior information of the target locations. The segmentation algorithm is useful to biological, natural, and textural pictures. As per the author the automatic version produces an average Tanimoto Coefficient (TC) result of 83.7 % meant for every thyroid US pictures in the record, whereas the empirical version attains a usual of 82.8 %.

Zhao et al. (69) watershed segmentation of thyroid images in the US was discussed. To provide a normalisation method, this study employs homomorphic filtering, anisotropic diffusion, and fractional differential. The Normalized Cut (NC) method designed by the researcher to analyze thyroid nodule subdivision in US pictures, that offered a precise position for thyroid nodules. Additionally, edge information from nodules improves fine needle aspiration cytology in evaluating thyroid nodule following segmentation for benign or cancerous.

## Conclusion

In this study of deep learning systems for US image segmentation, certain key concerns were addressed. All of these research used real-world data to show that the proposed technique worked in specific applications with small datasets. The question of why deep learning algorithms work for a specific problem is still open. The solution to this problem is currently a work in progress. Many scientists are developing new visual aids to help people grasp feature maps created from hidden layers more intuitively. That is the impact of an alteration in a data assembly device, subsequently variations in image attributes like brightness or colour intensity stages may result. Network performance will suffer as a result of the lack of generalizability. The demand for incredibly large image databases is another challenge with DLC networks. As a result, a lot of storage and memory will be required, as well as a large amount of training time for the networks.

Another important research area is the decrease of training time as well as the proper management of massive volumes of imaging data in terms of storage and memory requirements. DLC-based approaches for biological applications in clinical practise have also been hampered by a lack of large enough imaging datasets. Despite the fact that the healthcare industry has a vast amount of imaging data, it is not commonly shared since it contains protected health information is company's exclusive asset. As a result, efforts must be made to make such data agreeably accessible, whether over outstanding test struggles or facts offerings, because the longstanding paybacks of facts distribution outlying compensate every small time achievements obtained by keeping facts secreted.

From automated CT image segmentation to automated thyroid US image analysis, DL algorithms have empowered extraordinary accomplishment enrichments in a number of healthcare applications. However, if more captioned photographs are made publically available, more can be done. Manual labelling of visual figures by experts continues to be a substantial hurdle to ground truth generation. Unsupervised learning approaches should be given more attention in the absence of ground facts.

## References


1 Er, O., Sertkaya, C., Temurtas, F. and Tanrikulu, A.C., Journal of medical systems, **33(6)**, p. 485 (2009).
2 Vaz, V.A.S., International Journal of Innovative Research in Science, Engineering and Technology, **3(7)**, p. 14314 (2014).
3 Rivkees, S. and Bauer, A.J., In Sperling Pediatric Endocrinology p. 395 (2021).
4 Dayal, D. and Prasad, R., Res Rep Endocr Disord, **5(5)**, p. 91 (2015).
5 Dayal, D. and Gupta, B.M., Thyroid Research and Practice, **17(3)**, p.134 (2020).
6 Vemulapalli L, Sekhar PC., Indian Journal of Applied Research, 9, p. 398 (2019).
7 Masood, S., Sharif, M., Masood, A., Yasmin, M. and Raza, M., Current Medical Imaging, **11(1)**, p. 3 (2015).
8 Pal, A., Chaturvedi, A., Garain, U., Chandra, A., and Chatterjee, R., ICPR p. 1478 (2016).
9 Wang, G., IEEE, **4**, p. 8914 (2016).
10 da Silva, F.H.S., Deep learning for Corpus Callosum segmentation in brain magnetic resonance images (2018).

11 Volkenandt, T., Freitag, S. and Rauscher, M., Microscopy and Microanalysis, **24(S1)**, p. 520 (2018).
12 Işın, A., Direkoğlu, C. and Şah, M., Procedia Computer Science, **102**, p. 317 (2016).
13 Millioni, R., Sbrignadello, S., Tura, A., Iori, E., Murphy, E. and Tessari, P., Electrophoresis, **31(10)**, p. 1739 (2010).
14 Iglesias, J.E., International Conference on Information Processing in Medical Imaging, p. 610 (2017).
15 Fan, M. and Lee, T.C., IET image processing, **9(6)**, p. 478 (2015).
16 Fan, J., Wang, R., Li, S. and Zhang, C., 12th International Conference on Control Automation Robotics & Vision (ICARCV,) p. 877 (2012).
17 Kim, Y.J., Lee, S.H., Park, C.M. and Kim, K.G., Healthcare informatics research, **22(4)**, p. 305 (2016).
18 Roth, H.R., Shen, C., Oda, H., Oda, M., Hayashi, Y., Misawa, K. and Mori, K., Medical Imaging Technology, **36(2)**, p. 63 (2018).
19 Zhou, X., Yamada, K., Kojima, T., Takayama, R., Wang, S., Zhou, X., Hara, T. and Fujita, H., Medical Imaging : Computer-Aided Diagnosis, 10575, p. 105752 (2018).
20 Shen, D., Wu, G. and Suk, H.I., Annual review of biomedical engineering, **19**, p.221 (2017).
21 Yoon, D., Healthcare informatics research, **23(2)**, p.75 (2017).
22 Russell, S. and Norvig, P., Artificial intelligence: a modern approach (2002).
23 Yu, K.H., Beam, A.L. and Kohane, I.S., Nature biomedical engineering, **2(10)**, p.719 (2018).
24 Suzuki, K., Radiological physics and technology, 10(3), p. 257 (2017).
25 Deng, L. and Yu, D., Foundations and trends in signal processing, **7(3–4)**, p.197 (2014).
26 Shen, D., Wu, G. and Suk, H.I., Annual review of biomedical engineering, **19**, p.221 (2017).
27 Wang, G., IEEE, **4**, p.8914 (2016).
28 Suzuki, K., Radiological physics and technology, **10(3)**, pp.257 (2017).
29 Guo, Y., Liu, Y., Oerlemans, A., Lao, S., Wu, S. and Lew, M.S., Neurocomputing, **187**, p.27 (2016).
30 Krizhevsky, A., Sutskever, I. and Hinton, G.E., Advances in neural information processing systems, **25**, p.1097 (2012).
31 Garcia-Garcia, A., Orts-Escolano, S., Oprea, S., Villena-Martinez, V., Martinez-Gonzalez, P. and Garcia-Rodriguez, J., Applied Soft Computing, **70**, p.41 (2018).
32 Ronneberger, O., Fischer, P. and Brox, T., International Conference on Medical image computing and computer-assisted intervention p. 234 (2015).
33 Milletari, F., Navab, N. and Ahmadi, S.A., Fourth international conference on 3D vision (3DV), p.565 (2016).
34 N. I. of H.-C. Center. Chest X-ray NIHCC. [Online]. Available, https://nihcc.app.box.com/v/ChestXray-NIHCC [Accessed: 10-Nov-2021] (2017).
35 T. M. I. of T. (MIT)'s L. for C. Physiology. MIMIC-chest X-ray database (MIMIC-CXR) [Online]. Available, https://physionet.org/content/mimic-cxr/2.0.0/ [Accessed: 10-Nov-2021].
36 Reddy, U.M., Filly, R.A. and Copel, J.A., Obstetrics and gynecology, **112(1)**, p.145 (2008).

37 Haugen, B.R., Alexander, E.K., Bible, K.C., Doherty, G.M., Mandel, S.J., Nikiforov, Y.E., Pacini, F., Randolph, G.W., Sawka, A.M., Schlumberger, M. and Schuff, K.G., The American Thyroid Association guidelines task force on thyroid nodules and differentiated thyroid cancer, **26(1)**, pp.1(2016).

38 Gharib, H., Papini, E., Paschke, R., Duick, D.S., Valcavi, R., Hegedüs, L. and Vitti, P., Journal of endocrinological investigation, **33(5)**, p.287 (2010).

39 Kwak, J.Y., Han, K.H., Yoon, J.H., Moon, H.J., Son, E.J., Park, S.H., Jung, H.K., Choi, J.S., Kim, B.M. and Kim, E.K., A step in establishing better stratification of cancer risk. Radiology, **260(3)**, p. 892 (2011).

40 Park, J.Y., Lee, H.J., Jang, H.W., Kim, H.K., Yi, J.H., Lee, W. and Kim, S.H., A proposal for a thyroid imaging reporting and data system for ultrasound features of thyroid carcinoma. Thyroid, **19(11)**, p.1257 (2009).

41 Fotenos, A.F., Snyder, A.Z., Girton, L.E., Morris, J.C. and Buckner, R.L., Normative estimates of cross-sectional and longitudinal brain volume decline in aging and AD. Neurology, **64(6)**, p.1032 (2005).

42 Golan, R., Jacob, C. and Denzinger, J., International Joint Conference on Neural Networks (IJCNN), p. 243-(2016).

43 Milletari, F., Ahmadi, S.A., Kroll, C., Plate, A., Rozanski, V., Maiostre, J., Levin, J., Dietrich, O., Ertl-Wagner, B., Bötzel, K. and Navab, N., Computer Vision and Image Understanding, **164**, p.92 (2017).

44 Perez, L. and Wang, J., The effectiveness of data augmentation in image classification using deep learning. arXiv preprint arXiv:1712.04621.

45 Shie, C.K., Chuang, C.H., Chou, C.N., Wu, M.H. and Chang, E.Y., Transfer representation learning for medical image analysis. 37$^{th}$ annual international conference of the IEEE Engineering in Medicine and Biology Society (EMBC), p.711 (2015).

46 Garcia-Garcia, A., Orts-Escolano, S., Oprea, S., Villena-Martinez, V., Martinez-Gonzalez, P. and Garcia-Rodriguez, J., Applied Soft Computing, **70**, p. 41(2018).

47 Baratloo, A., Hosseini, M., Negida, A. and El Ashal, G., p.48 (2015).

48 Lalkhen, A.G. and McCluskey, A., Continuing education in anaesthesia critical care & pain, **8(6)**, p.221(2008).

49 Van Stralen, K.J., Stel, V.S., Reitsma, J.B., Dekker, F.W., Zoccali, C. and Jager, K.J., Kidney international, **75(12)**, p.1257 (2009).

50 Csurka, G., Larlus, D., Perronnin, F. and Meylan, F., BMVC, **27**, p. 10 (2013).

51 Wong, H.B. and Lim, G.H., Proceedings of Singapore healthcare, **20(4)**, p.316 (2011).

52 Xu, Y., Wang, Y., Yuan, J., Cheng, Q., Wang, X. and Carson, P.L., Ultrasonics, **91**, p.1 (2019).

53 Badea, M.S., Felea, I.I., Florea, L.M. and Vertan, C., arXiv preprint arXiv:1605.09612 (2016).

54 Kaur, J. and Jindal, A., International Journal of Computer Applications, **50(23),** p.1 (2012).

55 Poudel, P., Illanes, A., Sheet, D. and Friebe, M., Journal of healthcare engineering, (2018).

56 Shenoy, N.R. and Jatti, A., Indonesian Journal of Electrical Engineering and Computer Science, **21(3)**, p.1424 (2021).

57 Garg, H. and Jindal, A., Fourth International Conference on Computing, Communications and Networking Technologies (ICCCNT), pp.1 (2013).
58 Frannita, E.L., Nugroho, H.A., Nugroho, A. and Ardiyanto, I., 2nd International Conference on Imaging, Signal Processing and Communication (ICISPC), p. 79(2018).
59 Ying, X., Yu, Z., Yu, R., Li, X., Yu, M., Zhao, M. and Liu, K., International Conference on Neural Information Processing, p.373 (2018).
60 Xu, Y., Wang, Y., Yuan, J., Cheng, Q., Wang, X. and Carson, P.L., Ultrasonics, **91**, pp.1 (2019).
61 Ma, J., Wu, F., Zhu, J., Xu, D. and Kong, D., Ultrasonics, **73**, p.221 (2017).
62 Wu, K., Chen, X. and Ding, M., Optik, **125(15)**, pp.4057 (2014).
63 Perrin, D.P., Bueno, A., Rodriguez, A., Marx, G.R. and Pedro, J., Medical Imaging:Computer-Aided Diagnosis, **10134**, p.1013431(2017).
64 Yap, M.H., Pons, G., Martí, J., Ganau, S., Sentís, M., Zwiggelaar, R., Davison, A.K. and Marti, R., IEEE journal of biomedical and health informatics, **22(4)**, p.1218 (2017).
65 Song, W., Li, S., Liu, J., Qin, H., Zhang, B., Zhang, S. and Hao, A., IEEE journal of biomedical and health informatics, **23(3)**, p.1215 (2018).
66 Chang, C.Y., Hong, Y.C. and Tseng, C.H., 2011. IEEE Computational Intelligence Magazine, **6(4)**, p.43 (2011).
67 Gui, L., Li, C. and Yang, X., Physica Medica, **42**, pp.162(2017).
68 Mylona, E.A., Savelonas, M.A. and Maroulis, D., Springer Plus, **3(1)**, p.1 (2014).
69 Zhao, J., Zheng, W., Zhang, L. and Tian, H., Health information science and systems, **1(1)**, p.1(2013).